

Ultrafast nonlinear tuning of the reflection properties of AlGaAs photonic crystal waveguides by two-photon absorption

A. D. Bristow,^{a)} D. O. Kundys, A. Z. García-Déniz, J.-P. R. Wells, A. M. Fox,^{b)}
M. S. Skolnick, and D. M. Whittaker

Department of Physics and Astronomy, University of Sheffield, Sheffield, S3 7RH, United Kingdom

A. Tahraoui^{c)} and T. F. Krauss

School of Physics and Astronomy, University of St. Andrews, St. Andrews, KY16 9SS, United Kingdom

J. S. Roberts

Department of Electronic and Electrical Engineering, University of Sheffield, Sheffield, S1 3JD, United Kingdom

(Received 17 May 2004; accepted 20 July 2004)

We have studied the power-dependent wavelength shift of photonic coupling resonances of a two-dimensional photonic crystal waveguide by reflection geometry pump-probe measurements. The quadratic response is indicative of two-photon induced carrier creation, which alters the refractive index of the semiconductor core of the photonic lattice. A free-carrier model is used to simulate the phenomenon, giving values of the change in refractive index per unit carrier density that satisfactorily compare to values calculated for bulk AlGaAs under similar conditions. Time-resolved spectra are also presented, showing relaxation times of <10 ps which are consistent with surface recombination times in the patterned waveguide. © 2004 American Institute of Physics. [DOI: 10.1063/1.1790569]

I. INTRODUCTION

$\text{Al}_{1-x}\text{Ga}_x\text{As}$ planar waveguides patterned with two-dimensional (2D) hexagonal lattices of air holes provide band gaps in the electromagnetic (EM) spectrum. This phenomenon has attracted much attention due to the innovative way in which it can be used to control the propagation and emission of light.^{1,2} The incorporation of photonic band gap materials in state-of-the-art photonic telecommunication technologies has been the goal of many research groups worldwide for over a decade. The ability to use transferable growth and fabrication techniques from the field of semiconductor physics also opens up the possibility of including nonlinear interactions in the operation of these materials. Consequently, the properties of photonic crystals combined with semiconductor nonlinearities are of great importance and potentially offer a wealth of interesting effects.^{3–11} In particular, it is predicted that semiconductor photonic crystal should provide rapid all-optical switching and soliton formation as a result of the strong confinement and dispersion of the light.^{3–8} Despite this theoretical interest, experimental work on switching in high index-contrast photonic crystals has only recently become a reality.^{9–11}

We recently reported on nonlinear switching measurements in AlGaAs photonic crystal waveguides (PCWs), demonstrating that a free carrier induced change in refractive index can produce an enhanced change in the reflectivity close to a photonic resonance.¹¹ The nonlinear reflectivity

was observed to have a rise time of ~ 2 ps and a decay time of <10 ps. This decay time is more than an order of magnitude faster than that observed in bulk AlGaAs¹² and is thought to be determined by the surface recombination of the photogenerated carriers at the edges of the air holes. The enhanced nonlinearity and fast response time confirms the excellent potential of PCWs in nonlinear switching applications.

In this paper, we present power-dependent data with improved temporal resolution to clarify the origin of the nonlinearity, and outline a simple model to account for the magnitude of the wavelength shift. The results and the modeling together confirm that the wavelength shift originates from free carriers generated by two-photon absorption (TPA) in the AlGaAs core. We also present a preliminary study of the dependence of the nonlinear response on the excitation wavelength and the effect of incorporating quantum wells (QWs) into the waveguide core to enhance the nonlinearity. These studies indicate that there is considerable scope to optimize the nonlinear response, with the prospect of obtaining large nonlinearities at lower intensities, which is essential for realistic applications in photonic switching.

II. SAMPLES AND EXPERIMENTAL DETAILS

The PCW comprises of an asymmetric planar waveguide that is deeply etched with a 2D hexagonal lattice of air holes. The waveguide is grown by metal-organic vapor phase epitaxy on a GaAs substrate, which were orientated at 3° off of the [100] direction towards the [110] direction. It consists of an $\text{Al}_{0.2}\text{Ga}_{0.8}\text{As}$ core layer of thickness $d=400$ nm and a lower $\text{Al}_{0.6}\text{Ga}_{0.4}\text{As}$ cladding layer with thickness $d_{c1}=1500$ nm, as shown in Fig. 1. The top cladding layer is air

^{a)}Present address: Department of Physics, University of Toronto, Toronto M5S 1A7, Canada.

^{b)}Electronic mail: mark.fox@sheffield.ac.uk

^{c)}Present address: Department of Electronic and Electrical Engineering, University of Sheffield, Sheffield, S1 3JD, United Kingdom.

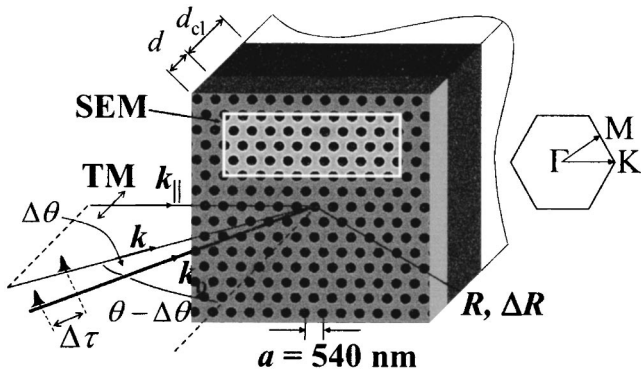


FIG. 1. Experimental geometry of the pump-probe spectroscopy technique. The layer structure of the sample is indicated, together with a scanning electron micrograph of the PCW surface. The corresponding Brillouin zone and crystal point symmetry are shown to the right.

with a thin (10 nm) capping layer to protect the surface from oxidation. The semiconductor wafer is patterned with a photonic crystal, $80 \times 80 \mu\text{m}^2$ in size surrounded by a $\sim 20 \mu\text{m}$ air moat. Patterning is achieved by electron-beam lithography and chemically assisted ion beam etching, which produces very vertical holes with an aspect ratio of 10:1. The lattice under investigation here has a period of $a = 540 \text{ nm}$ and hole radius of $r \approx 110 \text{ nm}$, and consequently an air-fill factor of $f \approx 30\%$. The etch depth in these structures is therefore comfortably larger than the thickness of the waveguide core, ensuring good confinement of the propagating modes. Note that incorporated into the schematic in Fig. 1 is a scanning electron micrograph of the top surface of the real PCW structure.

The PCW sample was characterized by external coupling reflectivity. The external radiation is coupled to propagating modes in the structure when the phase-matching condition

$$k_{\parallel} = \frac{\omega}{c} \sin \theta \quad (1)$$

is achieved, where k_{\parallel} is the in-plane \mathbf{k} -vector, ω is the angular frequency of the external radiation, and θ is the angle of incidence. This method examines the leaky modes from the structure which present themselves as minima, maxima or Fano-like resonances in the reflectivity spectra.¹³ A set of angle-tuned measurements is used to extract the portion of the photonic band structure that lies above the light line. Typical spectra are presented in Sec. III.

Time-resolved pump-probe experiments were performed with a weak white-light laser continuum as the probe, and a high-intensity laser beam as the pump. The pump pulse, with wave vector \mathbf{k}_p , has a variable delay between it and the probe pulse (with wave vector \mathbf{k}), allowing a small time difference ($\Delta\tau$) to be introduced into the experiment, as indicated in Fig. 1. Time-resolved pump-probe spectroscopy measurements of this sort can be used to examine the temporal dynamics and the profile of the coupling resonance for a variety of different excitation conditions. In the data presented in the following section, the power-dependent nature of the spectra are studied for $\Delta\tau = 0$, i.e., this occurs when the blueshift of

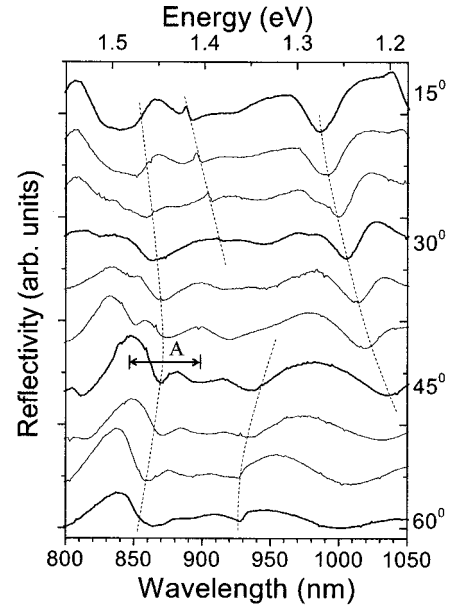


FIG. 2. Angle-tuned reflectivity spectra along the Γ - K direction of the hexagonal 2D lattice PCW with TM polarization. The region marked A corresponds to the spectral region studied in the reflection geometry pump-probe measurements.

the photonic resonance under investigation is at a maximum. In this setup both beams are incident on the sample surface with an angular difference of $\Delta\theta \approx 6^\circ$.

The laser source is a 1 kHz Ti:sapphire regenerative amplifier, tuneable around 800 nm with a pulse width of $\tau_p = 150 \text{ fs}$ which is split into the pump and probe beams by a 75:25 beam splitter. The pump path includes a delay stage and is incident on the sample with weak focusing by a 25 cm lens to a spot size of $\sim 200 \mu\text{m}$. The long focal length lens increases the Rayleigh range of the focused pump beam close to the sample and minimizes the angular divergence. The probe beam is tightly focused on a 1 mm thick sapphire plate (attenuated to $< 1 \mu\text{J}$ per pulse)¹⁴ that generates a single filament white-light continuum¹⁵ via self-phase modulation. The probe continuum is then collimated with a spot size of $< 2 \text{ mm}$ and a divergence of $< 1^\circ$. The probe light is directed towards the sample wafer, the reflection of which is spatially filtered¹¹ to select light from only the photonic crystal under investigation. The reflected signal is then coupled into a spectrometer with a thermoelectrically cooled charge-coupled device (CCD) attached. A reference beam from the white-light continuum is also coupled into the spectrometer, the CCD is binned vertically into two stripes so that the reflected signal can be normalized against the reference. The normalization removes any variation due to instabilities in the white-light continuum and improves the signal-to-noise ratio (SNR) by more than an order of magnitude. The SNR is also improved by acquiring 20 accumulations per spectra with the CCD.

III. EXPERIMENTAL RESULTS

Figure 2 shows a typical set of angle-tuned ($15^\circ \leq \theta \leq 60^\circ$) linear reflectivity spectra along the Γ - K direction for *transverse-magnetic* (TM) polarization in which the mag-

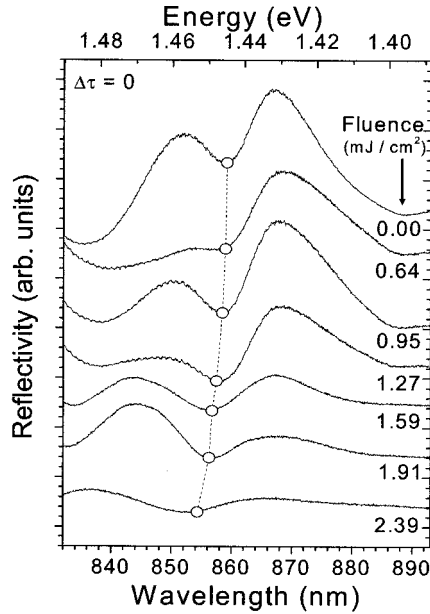


FIG. 3. Pump-probe reflectivity spectra for $\Delta\tau=0$ over a range of $0 \leq \text{fluence} \leq 2.39 \text{ mJ/cm}^2$ with $\lambda_{\text{pump}}=800 \text{ nm}$. The reflection spectra show a photonic coupling feature at 860 nm which blueshifts increasingly with greater power.

netic field lies in the plane of the waveguide. The spectra consist of broad Fabry-Perot oscillations with sharper photonic features superimposed on top of them. The Fabry-Perot oscillations originate from the thin film interference between the surface and the interfaces within the structure, and have negligible effect on the following results. The photonic features, on which we concentrate here, are either Fano-like or minima, and are identified with dashed lines in Fig. 2. We concentrate on the $\theta=45^\circ$ spectrum, which has a coupling feature at $\sim 860 \text{ nm}$ with a minimum in the reflectivity. The region of the spectra which includes this resonance, labeled A in the figure, will be used to perform the nonlinear measurements described in Fig. 3.

Figure 3 shows the results from the pump-probe experiment for the 860 nm coupling feature in the 45° spectrum for $\Delta\tau=0$ as a function of pump power dependence with $\lambda_{\text{pump}}=800 \text{ nm}$. Zero delay time corresponds to the maximum excitation when the pump and probe beams overlap temporally, hence providing the maximum wavelength shift at each power. The range of $0 \leq \text{fluence} \leq 2.39 \text{ mJ/cm}^2$ is presented in the figure. The zero fluence spectrum (top) is obtained by setting the time delay to negative values significantly larger than the pulse width of the laser; consequently the probe beam arrives at the sample before the pump. The coupling feature at 860 nm is visible and comparable to that observed in region A of Fig. 2. At nonzero fluences the photocreated free-carrier density alters the refractive index of the semiconductor region and hence the photonic band structure. This results in a blueshift of the photonic coupling resonance that increases with increasing fluence, as shown in Fig. 3.

The amplitude of the blueshift deduced from Fig. 3 is shown in Fig. 4 as a function of pump fluence. The intensity [defined in Eq. (5)] and the change in refractive index are marked on the opposite axes. The latter is deduced from the approximate relationship

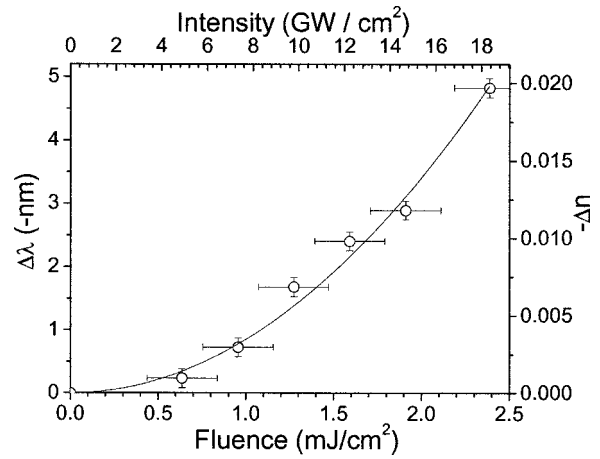


FIG. 4. Blueshift of the 860 nm coupling feature as a function of average pump fluence in the range $0 \leq P_{\text{ave}} \leq 2.39 \text{ mJ/cm}^2$. The intensity and the refractive index change deduced from Eq. (2) are marked on the opposite axes. The solid line is a quadratic fit with $\Delta\lambda \propto I_0^2$.

$$\Delta n = n_0 \frac{\Delta\lambda}{\lambda_0}, \tag{2}$$

where λ_0 and n_0 are the linear wavelength and refractive index, respectively. The justification for this approximation is discussed in Sec. IV. The strength of the blueshift is comparable with that observed in our previous work.¹¹ The power-dependent measurements reveal that the amplitude of the wavelength shift follows a square law dependence on the pump beam intensity. This is illustrated by the solid line in Fig. 4, which represents a fit of $\Delta\lambda$ (and hence Δn) $\propto I_0^2$. The details are also discussed in Sec. IV.

In Fig. 5 a color contour plot of the experimental reflectivity spectra is presented as a function of both wavelength and time delay for the fluence of 1.59 mJ/cm^2 . In the figure red represents high and blue represents low reflectivity, respectively. The striping effect is a result of the plot being constructed from multiple spectra which are normalized and averaged by the method described in Sec. II. The change in the central position of the photonic coupling resonance at $\lambda_0 \sim 860 \text{ nm}$ is overlaid. The rise time is close to 2 ps, which

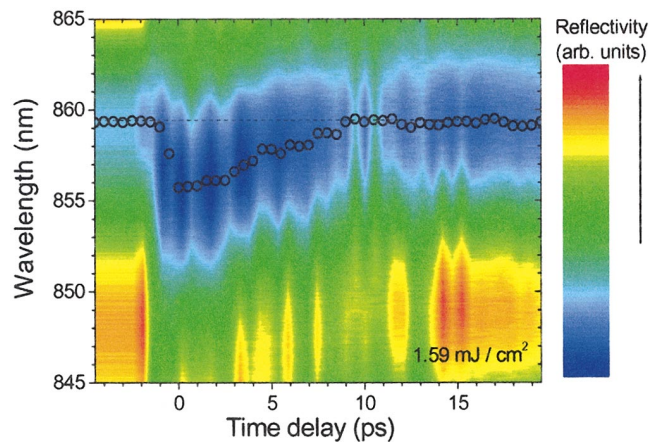


FIG. 5. (Color) Color contour plot of the reflectivity as a function of both wavelength and time delay. Overlaid is the central position of the photonic coupling feature (black circles).

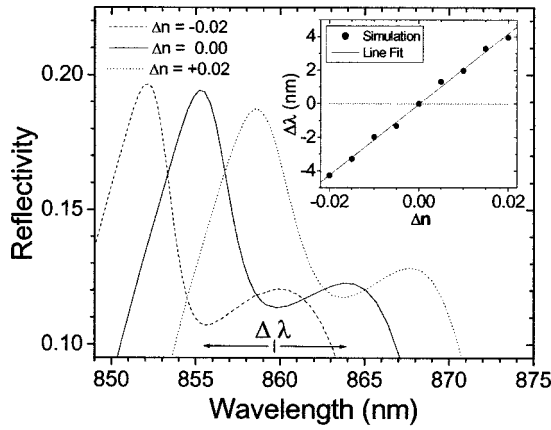


FIG. 6. Simulated reflection spectra for $\Delta n = 0.00, \pm 0.02$ showing the expected direction and magnitude of the nonlinear shift observed. The inset shows the dependence of the minimum in the reflectivity as a function of the change in the refractive index of the semiconductor core.

is shorter than the temporal resolution in our previous results. In this experiment the pump excitation is at $0.95 \times E_g$, consequently TPA excites carriers high into the conduction band. The observed excitation will therefore be effected by intervalley scattering and carrier cooling, which occur on the same time scale.¹⁶ From Fig. 5 the $1/e$ decay time for this power is ≈ 7 ps. This closely matches the results obtained previously, where the decay time was an order of magnitude faster than that observed in bulk AlGaAs (~ 100 ps) under similar conditions.¹² This is due to the deep etching and hence the increased surface recombination. For each of the other powers in the series presented in Fig. 3, the relaxation time is also very similar to this value, with a deviation that is within experimental errors. Consequently, there appears to be no carrier density dependence of the decay time.

IV. MODELING

The linear relationship given in Eq. (2) is verified by studying the effect of altering the refractive index of the semiconductor region in a theoretical simulation of the reflectivity of the photonic lattice. This is modeled by using a steady-state scattering-matrix method simulation¹⁷ of the reflectivity for different values of the refractive index over a range corresponding to $-0.02 \leq \Delta n \leq +0.02$. Figure 6 shows the calculated spectra for the two extremes compared with the reference $\Delta n = 0$ (solid curve). For a Δn of -0.02 (dashed curve) the photonic coupling resonance at ~ 860 nm undergoes a blueshift of ≈ 4.5 nm, which coincidentally is comparable with the experimental observation. The inset to Fig. 6 shows the dependence of the wavelength shift as a function of the change in refractive index. The relationship is approximately linear and the gradient extracted from the figure is 211 nm per unit index change, which is comparable to the value of $\lambda_0/n_0 \approx 245$ nm used in the determination of Δn from Eq. (2) in Fig. 4.

We now discuss the nonlinear behavior in terms of a steady-state approximation of the carrier creation due to the incident radiation. From simple free-carrier models for TPA

in GaAs-based materials,^{18–20} it can be shown that the change in refractive index is proportional to the square of the intensity. This follows because

$$\Delta n = \sigma N, \quad (3)$$

σ being the change in refractive index per unit carrier density and N the number of carriers, which is proportional to I_0^2 through²⁰

$$N = \frac{\beta I_0^2 \tau_p}{2\hbar\omega_p} \sqrt{\frac{\pi}{2}}, \quad (4)$$

where $\beta = 3.1 \times 10^{-8}$ cm/W is the TPA coefficient²¹ and ω_p is the angular frequency of the pump pulse. In this case the pump beam is defined as

$$I(r, t) = I \exp(-t^2/\tau_p^2) \exp(-2r^2/w_0^2), \quad (5)$$

where t is the time, r is the radial distance, τ_p is the pulse width, and w_0 is the beam waist at the sample. The intensity range used in the experimental results presented here excites between 10^{18} and 10^{19} carriers per cubic centimetre.

A quadratic curve is drawn onto the data points in Fig. 3 from which the change of refractive index per unit carrier density can be extracted. This is achieved by dividing the quadratic fit to Δn by the square of the pump intensity, to find $\Delta n/I_0^2$, and then substituting Eq. (4) into Eq. (3) to obtain $\sigma = -3.5 \pm 1.4 \times 10^{-20}$ cm³. This method allows for the comparison between the theoretical values of the free carriers induced index change for patterned and unpatterned AlGaAs, where σ is defined as¹⁹

$$\sigma = \frac{e^2}{2\omega_{pr}^2 \epsilon_0 n_0 m_{\text{eff}}} \frac{E_g^2}{E_g^2 - (\hbar\omega_p)^2}, \quad (6)$$

where ω_{pr} is the angular frequency of the probe beam, m_{eff} is the reduced effective mass of the carriers and $E_g = 1.7$ eV is the electronic band gap of the waveguide core. Equation (6) at $\hbar\omega_p \sim 0.95 \times E_g$ gives $\sigma = -0.7 \pm 0.1 \times 10^{-20}$ cm³, which matches the values presented in the literature for bulk AlGaAs under similar conditions,^{18,19} and differs by only a factor of 4 from that obtained in our experiment. One possible reason for the discrepancy is that Eq. (6) does not take account of excitonic enhancements close to the band edge of the Al_{0.2}Ga_{0.8}As waveguide core or band-edge renormalization. Nevertheless, one clear conclusion is that the quadratic dependence confirms that TPA is the dominant nonlinear process involved in the blueshift of the photonic reflection feature.

The decay rate for carriers in this structure is modified from the bulk. The waveguide is patterned with a lattice of air holes which increase the surface area by more than a factor of 3. The surface recombination velocity for carrier densities of $10^{18} - 10^{19}$ cm⁻³ is $\sim 2 \times 10^6$ cm s⁻¹ in GaAs.²² The surface of the hexagonal unit cell is 540 nm wide and has air holes that have a radius of ~ 110 nm. If only the core region is considered, then a carrier has to travel a mean distance of ≈ 200 nm in any direction before reaching an interface where it can recombine. This leads to an estimation of

the surface recombination rate in the patterned waveguide of $(\sim 10 \text{ ps})^{-1}$, which is in agreement with the 7–8 ps relaxation times observed in our experiments.

V. DISCUSSION

The experimental conditions that we have employed here establish general principles of using PCWs in nonlinear photonic applications, but they are far from optimized; for instance, the intensities used in this work are extremely large compared to those required for a practical device. Hence, there is considerable scope for enhancing the effects that we have observed. In this section we give a qualitative discussion of two approaches to increase the magnitude of the effective nonlinearity, and also discuss the ways to increase the switching speed. Both of these are obvious requirements for eventual applications in ultrafast photonic switching with lower pump intensities.

The first method to enhance the effective nonlinearity is to couple the external pump radiation more efficiently through a coupling resonance of the photonic band structure. The experimental results presented so far in this paper are for a pump wavelength that is nonresonant with any photonic band structure modes. The wavelength of the pump beam can be tuned so that it is overlapped with a photonic coupling resonance, consequently resulting in phase matching of the pump light and stronger coupling to the waveguide core. The increased intensity in the coupled mode leads to an increase in the population of photogenerated carriers for the same incident power. In this structure a photonic band structure mode at 794 nm is observed in the reflectivity. The EM energy density was calculated by steady-state scattering-matrix simulations for this photonic mode. The intensity of the probe light coupled into the mode as a function of wavelength across the feature is calculated to enhance by approximately three times exactly on resonance compared to a detuning of only 10 meV. Preliminary pump-probe experiments were performed altering the wavelength of the pump light and observing the blueshift of the coupling resonance at 860 nm, as before. The results indicate a doubling of the observed blueshift when the pump wavelength is closest to the 794 nm resonance, thus confirming the general trend of the calculations. Further experiments to establish the quantitative enhancement due to pump coupling considerations are required, along with a time-dependent theoretical comparison. Also we expect that enhancement can be achieved by coupling the external radiation into a band with a very flat dispersion, i.e., a defect band.

The second method by which the blueshift can be enhanced is to alter the properties of the material from which the PCW is made. For comparison to the data presented here on passive waveguides, similar structures were fabricated which contained five evenly spaced InAlGaAs QWs with a band gap close to the pump wavelength to provide a resonant nonlinearity. Initial experiments show that over a very similar power range to that presented in Fig. 3 the photonic coupling feature undergoes a large blueshift up to $\sim 16 \text{ nm}$, limited by the damage threshold of the material. This result was

obtained without attempting to overlap the QW resonance with a photonic coupling resonance, which is expected to further enhance the observed phenomenon.

Fast all-optical switches require both fast switch-on and switch-off times. The faster the switch-on time the better the discrimination between the on and off states. The faster the switch-off time the higher the frequency at which the switch can operate. In optical switches where carrier excitation is the nonlinear mechanism then the recombination determines the switch-off time. In our structures the relaxation is $< 10 \text{ ps}$ and is dominated by the recombination at the surface, allowing a modulation frequency of up to $\sim 100 \text{ GHz}$. As the relative surface area is increased the time for the carriers to reach the surface is reduced and so faster switch-off times would be expected for smaller periods and larger air-fill factors. The switching time can be further reduced by changing to the regime where the optical switching is pulse width limited, either by excitation of a Kerr or AC Stark effect.⁹ In AlGaAs-based materials this can be achieved by pumping below the one- and two-photon absorption edges to excite virtual carriers.

VI. CONCLUSION

In summary, we exploit the coupling resonances observed in the band structure for 2D PCWs to demonstrate ultrafast all-optical nonlinear switching. By pumping close to the band gap of the AlGaAs waveguide core, free carriers are photogenerated. The induced free-carrier density in the semiconductor region of the lattice alters its refractive index, and hence the photonic band structure related to the periodic patterning. This manifests itself as a blueshift of the coupling resonance, showing a large change in the reflectivity close to the photonic feature.

The decay time of the observed blueshift shows that carriers are being excited from the valence to the conduction band. The power-dependent measurements show that the excitation has a square law dependence on the intensity of the incident pump light, which as the modeling confirms, is a result of two-photon absorption. The temporal measurements show that the relaxation process is not pulse width limited and that the observed decay time is due to surface effects both from the waveguide and the photonic patterning.

The temporal dynamics of the nonlinear effect show that the material nonlinearity is modified in terms of its decay time with respect to unpatterned material, which is governed by surface recombination. The photonic patterning reduces the switch-off time of the device, allowing for extremely fast operation speeds. We also discuss initial experimental results for further optimisation of the optical-switching process by the use of resonant pumping to either photonic band structure modes or buried quantum wells.

ACKNOWLEDGMENT

This work was funded by the EPSRC Grant Nos. GR/M72951 and GR/M22529.

¹T. F. Krauss, R. M. De La Rue, and S. Brand, *Nature (London)* **383**, 699 (1996).

²J. D. Joannopoulos, P. R. Villeneuve, and S. Fan, *Nature (London)* **386**,

- 143 (1997).
- ³M. Scalora, J. P. Dowling, C. M. Bowden, and M. J. Bloemer, *Phys. Rev. Lett.* **73**, 1368 (1994).
- ⁴Q. Li, C. T. Chan, K. M. Ho, and C. M. Soukoulis, *Phys. Rev. B* **53**, 15577 (1996).
- ⁵P. R. Villeneuve, D. S. Abrams, S. Fan, and J. D. Joannopoulos, *Opt. Lett.* **21**, 2017 (1996).
- ⁶P. M. Johnson, A. F. Koenderink, and W. L. Vos, *Phys. Rev. B* **66**, 081102 (2002).
- ⁷S. Lan and H. Ishikawa, *J. Appl. Phys.* **91**, 2573 (2002).
- ⁸M. G. Banaee, A. R. Cowan, and J. F. Young, *J. Opt. Soc. Am. B* **9**, 2224 (2002).
- ⁹M. Shimizu and T. Ishihara, *Appl. Phys. Lett.* **80**, 2836 (2002).
- ¹⁰S. W. Leonard, H. M. Van Driel, J. Schilling, and R. B. Wehrspohn, *Phys. Rev. B* **66**, 161102 (2002).
- ¹¹A. D. Bristow *et al.*, *Appl. Phys. Lett.* **83**, 851 (2003).
- ¹²M. J. LaGasse, K. K. Anderson, C. A. Wang, H. A. Haus, and J. G. Fujimoto, *Appl. Phys. Lett.* **56**, 417 (1990).
- ¹³See for example V. N. Astratov, I. S. Culshaw, R. M. Stevenson, D. M. Whittaker, M. S. Skolnick, T. F. Krauss, and R. De La Rue, *IEEE J. Lightwave Technol.* **17**, 2050 (1999); A. D. Bristow, V. N. Astratov, R. Shimada, I. S. Culshaw, M. S. Skolnick, D. M. Whittaker, A. Tahraoui, and T. F. Krauss, *IEEE J. Quantum Electron.* **38**, 880 (2002).
- ¹⁴M. K. Reed, M. K. Steiner-Shepard, M. S. Armas, and D. K. Negus, *J. Opt. Soc. Am. B* **12**, 2229 (1995).
- ¹⁵R. L. Fork, C. V. Shank, C. Hirlimann, R. Yen, and W. J. Tomlinson, *Opt. Lett.* **8**, 1 (1983).
- ¹⁶J. Shah, *Ultrafast Spectroscopy of Semiconductors and Semiconductor Nanostructures*, 2nd Ed. (Springer, Berlin, 1999).
- ¹⁷D. M. Whittaker and I. S. Culshaw, *Phys. Rev. B* **60**, 2610 (1999).
- ¹⁸I. Androsch and P. Glas, *Opt. Commun.* **105**, 125 (1994).
- ¹⁹T. G. Ulmer, R. K. Tan, Z. Zhou, S. E. Ralph, R. P. Kenan, C. M. Verber, and A. J. SpringThorpe, *Opt. Lett.* **24**, 756 (1999).
- ²⁰H. Folliot, M. Lynch, A. L. Bradley, T. Krug, L. A. Dunbar, J. Hegarty, J. F. Donegan, and L. P. Barry, *J. Opt. Soc. Am. B* **19**, 2396 (2002).
- ²¹H. Q. Le, H. K. Choi, and C. A. Wang, *Appl. Phys. Lett.* **57**, 212 (1990).
- ²²D. E. Aspnes, *Surf. Sci.* **132**, 406 (1983).